Comparison of partial structures of melts of superionic AgI and CuI and non-superionic AgCl

2007 J. Phys.: Condens. Matter 19 335201

(http://iopscience.iop.org/0953-8984/19/33/335201)

IOP PUBLISHING JOURNAL OF PHYSICS: CONDENSED MATTER

J. Phys.: Condens. Matter **19** (2007) 335201 (16pp) doi:10.1088/0953-8984/19/33/335201

Comparison of partial structures of melts of superionic AgI and CuI and non-superionic AgCl

Yukinobu Kawakita[1], **Shuta Tahara**[2,4], **Hiroyuki Fujii**[2,3], **Shinji Kohara**[3] **and Shin'ichi Takeda**[1]

[1] Department of Physics, Faculty of Sciences, Kyushu University, 4-2-1 Ropponmatsu, Fukuoka 810-8560, Japan
[2] Department of Condensed Matter Chemistry and Physics, Graduate School of Sciences, Kyushu University, 4-2-1 Ropponmatsu, Chuo-ku, Fukuoka 810-8560, Japan
[3] Research and Utilization Division, Japan Synchrotron Radiation Research Institute (JASRI, SPring-8), 1-1-1 Koto, Sayo-cho, Sayo-gun, Hyogo 679-5198, Japan

Received 11 May 2007, in final form 13 May 2007
Published 4 July 2007
Online at stacks.iop.org/JPhysCM/19/335201

Abstract

Neutron and high-energy x-ray diffraction analyses of molten AgI have been performed and the partial structures are discussed in detail with the aid of the structural modelling procedure of the reverse Monte Carlo (RMC) technique by comparison with those of molten CuI and AgCl. It is well known that AgI and CuI have a superionic solid phase below the melting point, in which the cations favour a tetrahedral configuration, while solid AgCl has a rock-salt structure with an octahedral environment around both Ag and Cl atoms. Even in the molten states, there is a significant difference between superionic and non-superionic melts. The cation is located on the triangular plain formed by three iodine ions in molten AgCl and CuI, while molten AgCl favours a 90° Cl–Ag–Cl bond angle, which is understood to maintain a similar local environment to that in the solid state. The atomic configurations of the RMC model suggest that the cation distributions in superionic melts of CuI and AgI exhibit large fluctuations, while Ag ions in the non-superionic melts of AgCl are distributed much more uniformly.

1. Introduction

Since an extremely flat Cu–Cu correlation for molten CuCl was reported [1, 2], molten structures of cuprous halides have been attracting many researchers' attention [3–12]. In earlier work aiming at the deduction of partial structures of binary liquids, the isotope substitution technique in neutron diffraction was often used. Three partial structures for a binary liquid can be solved numerically from three independent total structures for sample materials chemically identical with different content of isotope. Page and Mika [1] proposed the partial structures for molten CuCl as determined by this technique and suggested that the Cu–Cu partial pair

[4] Present address: Niigata University of Pharmacy and Applied Life Science, Higashijima, Akiha-ku, Niigata 956-8603, Japan.

distribution function is extremely flat and resembles that of a gas, which is completely different from the cation–cation partial pair distribution in typical molten salts such as molten alkali halides [13].

However, McGreevy and Pusztai [4] pointed out that numerically exact solutions obtained from three independent structural data sets do not always provide physically reasonable partial structures. The reverse Monte Carlo (RMC) simulation developed by them [14] is a convenient tool for constructing a structure model from several structural data sets under physically reasonable constraints. They suggested that, under the constraint of a reasonable cut-off length, that is, the minimum distance between two atoms that approach each other, the flat pair distribution of the Cu–Cu correlation cannot be reproduced and the Cu–Cu distribution obtained under this constraint has a prominent peak.

On the other hand, the Cu–Cu correlation in molten CuI has a characteristic first sharp diffraction peak (FSDP) in the partial structure factor and the Cu–Cu pair distribution penetrates into the nearest-neighbour shell corresponding to the unlike-pair correlation [9, 12]. The analysis of x-ray absorption fine structure (XAFS) also supports this Cu–Cu distribution, which is located at a slightly longer distance [10] than that in the RMC analysis of anomalous x-ray scattering (AXS) data [9]. Such penetration could not be predicted by earlier molecular dynamics (MD) simulation [3].

For molten CuBr, Allen and Howe [6] proposed an extremely flat Cu–Cu distribution function similar to that of molten CuCl [1] on the basis of the results of neutron diffraction analysis with the isotope substitution technique. Regarding this characteristic flat Cu–Cu correlation, Pusztai and McGreevy [7] again suggested that such a solution for partial structures is physically not acceptable because it violates the reasonable cut-off constraints. Saito *et al* [8] proposed a structural model generated by RMC simulation based on AXS spectra, where a more structured Cu–Cu pair distribution was demonstrated, although they insisted upon a similarity between CuCl and CuBr.

The flat Cu–Cu pair distribution function has been fascinating to researchers in relation to the fast ion conducting behaviour. CuBr and CuI exhibit superionic conducting behaviour at high temperature before melting [15]. CuCl does not show this property [15], although the superionic conducting phase has been found under high pressure [16]. In general, when materials melt, the bonding nature among constituents is enhanced by the lack of long-range order. However, recent *ab initio* MD simulations for molten and superionic CuI by Shimojo *et al* [11, 17] revealed that a more covalent picture of the bond is proper. Moreover, they suggested that, in addition to the unlike pair, even Cu–Cu has a bond with slight covalency, on the basis of the analysis of the bond overlap population, which is enhanced in the molten state [11]. Taking into account the covalent effect in ionic liquids sometimes sheds light on the dynamical properties for not only molten oxides but also chlorides such as molten $ZnCl_2$ [18]. Such covalent effects make ionic liquids viscous. In contrast to such a viscous liquid, Cu–Cu covalency may assist the cooperative motion of Cu ions in molten CuI, which may result in a several times larger diffusion constant of Cu ions than that of I ions [11].

In contrast to the featureless structure of Cu–Cu for molten CuCl, the experimental Ag–Ag correlation for molten AgCl obtained by the isotope substitution technique in neutron diffraction experiment has a strongly structured distribution [19] which seems unrealistic. The theoretical approaches for molten silver halides were directed toward reproducing the experimental total structure [19–21] by MD simulation through the refinement of the pair potential. Wilson *et al* [22] pointed out a possibility that the different properties between AgCl and alkali halides can be accounted for by the effects of polarization. They suggested that the three-peak fine structure of the main peak in the structure factor can only be a result of polarized ion potentials of Cl ions. Trullàs *et al* [23] and Bitrián and Trullàs [24] also

confirmed this anion-induced polarization effect on the structures for molten AgCl and AgBr. They found that the polarized Vashishta–Rahman (pVR) potential for unlike-ion pairs exhibits results closer to the experimental results than the other potential that they examined. It is worth mentioning that the partial structure factor for Ag–Ag has a characteristic hump beyond the first peak when polarized ion potentials are used, which is also observed in experimentally obtained partial structures for molten AgBr [25] and AgCl [26]. The mean square displacement for each ion, which was calculated using the pVR potential, exhibits a similar tendency to that of the superionic melt of AgI; this is different from that of any typical ionic melt such as alkali halides.

The purpose of our present study is to reveal how different the structure in local and medium ranges is between superionic and non-superionic melts and what the characteristic features are in the partial structures of the superionic melt. Recent developments of the high-energy x-ray diffraction (HEXRD) method and neutron diffraction (ND) using a pulsed source enable us to obtain more precise structural information with sufficient statistics in a wide momentum transfer range. From these data, partial structures can be easily determined with the help of structural modelling procedures. We present, in this paper, the results of x-ray and neutron diffraction measurements for molten AgI and discuss the partial structures of molten AgI in comparison with those of molten CuI and AgCl which have been recently published [12, 26].

2. Experimental procedure

2.1. High-energy x-ray diffraction

HEXRD measurements for molten AgI have been carried out at 660 °C using a two-axis diffractometer installed at the BL04B2 beamline [27] in the third-generation synchrotron radiation facility SPring-8, Hyogo, Japan. The incident x-ray beam was 113.26 keV in energy and 0.1093 Å in wavelength from a Si(111) monochromator with the third harmonic reflection. High-energy incident x-rays not only allow us to access a wide momentum transfer, Q, range, but also lead to significantly improved reliability of the obtained structure factor because of the increase in the amount of the irradiated sample and the decrease in the scattering contributions of the sample container and background, including air scattering, relative to the total scattering intensity. The scattering intensities were measured by using a Ge solid-state detector in transmission geometry. A sample with a purity of 99.5% was sealed in a fused silica capillary with an inner diameter of 2.4 mm⌀ and wall thickness of 0.45 mm⌀. The sample capillary was located in the chamber filled with 1 atm He. High temperatures were achieved by heating with a Mo resistance wire of 0.5 mm diameter.

The diffraction pattern was obtained with the angle interval of 0.025° for the small-angle region from 0.3° to 5°, 0.050° for the middle-angle region from 4° to 12°, and 0.10° for the large-angle region from 11° to 25°. The accessible momentum transfer was from 0.3 to 24.8 Å^{-1}. Taking into account statistical accuracy, appropriate incident and receiving slits and measuring time per step were chosen for each angle range, so that the typical accumulated counts were 8×10^4 at the first peak position in the structure factor, 1.5×10^5 for the middle-angle range and 2×10^5 for the high-angle range. The total statistical error was estimated to be within 0.36%. The background contribution, including the scattering from the empty capillary, was less than 1/3 at the momentum transfer of 1 Å^{-1} and 1/5 at the first peak region in the obtained structure factor.

2.2. Neutron diffraction

We have carried out neutron diffraction measurements for molten AgI at 660 °C using the HIT-II spectrometer [28] installed at KENS, the pulse neutron facility of the High Energy

Accelerator Research Organization, KEK, Tsukuba, Japan. The sample was sealed in a thin-walled cylindrical container made of fused silica under Ar gas of 1 atm to avoid decomposition of the sample at high temperatures. The size of the container was 8 mm in inner diameter for molten AgCl and AgI and 10 mm for molten CuI, 0.3 mm in wall thickness and 140 mm in coaxial length. The neutron beam was collimated so as to irradiate 50 mm length of the sample. High temperatures were achieved with an infrared imaging furnace. HIT-II is a time-of-flight (TOF) diffractometer in which neutrons scattered by the sample are counted by fixed detectors in a time series from the trigger of a pulse of the neutron source.

In order to extract the structure factor, $S(Q)$, from the measured neutron intensity, $I(Q)$, normalization of the wavelength distribution in the incident neutron flux, subtraction of the scattering contribution from the cell taking into account neutron absorption by the sample and the cell, and multiple scattering correction were carried out [29]. The absorption factors for cylindrical cells were calculated by the method proposed by Paalman and Pings [30], and multiple scattering terms were obtained by the method of Blech and Averbach [31]. Atomic coherent and incoherent cross sections are obtained from the tables given by Sears [32].

For TOF analysis, the neutron-wavelength dependence of the absorption cross section should be known. Usually, the absorption cross section is proportional to the neutron wavelength. However, on approaching the wavelength where resonance absorption takes place, this proportional relation starts failing. In this epithermal wavelength region, the transmittance of the neutron beam is very high compared with that of a thermal neutron beam, and provides us with a good scattering condition of low absorption and low multiple scattering. The Ag atom has a resonance absorption at 5.19 eV corresponding to the wavelength of 0.0126 Å, and the proportional relation starts failing from around 0.4 Å. In this experiment, the wavelength dependence of Ag absorption was estimated by measuring a vanadium standard sample under the condition that the incident beam passed through Ag plates of 1 and 3 mm thickness.

Although the TOF method yields diffraction patterns with good statistics over a wide Q region, the Q resolution is relatively low, $\Delta Q/Q \sim 0.0694$, at the lowest scattering angle for HIT-II spectrometer. Also, the accessible Q minimum is around 0.7 Å^{-1}, which is too large for discussing the medium-range order of the structure. We have performed a complementary experiment for a low-Q region. Angular dispersive neutron diffraction with a fixed wavelength 1.82 Å of the incident neutron beam was carried out using the HERMES spectrometer at the reactor JRR-3M of the Japan Atomic Energy Agency (JAEA) in Tokai, Japan. The sample was sealed in the same container as that used in the TOF experiment. A high temperature was achieved using a conventional Nicrome wire heater.

The accumulation counts for the TOF experiment using the HIT-II spectrometer was 2×10^8 in the Q region from 1.6 to 2.4 Å^{-1}. On the other hand, the maximum count for the angular dispersive experiment using HERMES is around 1×10^5 at the first peak of the structure factor. The total statistical error for the combined structure factor was estimated to be within 0.96%.

3. Experimental results

The total structure factors of molten AgI obtained by neutron and x-ray diffraction analyses exhibit different intensity profiles from each other for the hump located at around $Q = 1$ Å^{-1} and the spike like feature at $Q = 1.9$ Å^{-1}, as shown in figure 1. These differences originate from the difference in the scattering abilities of x-ray and neutron beams between Ag and I atoms. For neutron diffraction, the coherent scattering length of Ag is slightly larger than that of I (Ag: 5.922 fm, I: 5.28 fm), so the scattering intensity emphasizes the correlation including Ag ions. On the other hand, the number of electrons in the I atom is slightly larger than that in

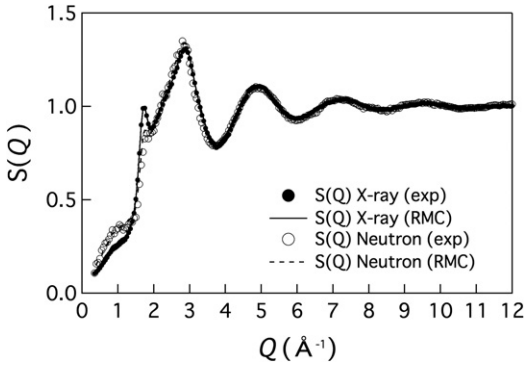

Figure 1. Total structure factors for molten AgI at 650 °C obtained by x-ray (solid circles) and neutron (open circles) diffraction analyses and the results of the RMC fits to both spectra (x-ray: solid line, neutron: chain lines).

Table 1. Contributions of three partial structure factors in total structure factors obtained by x-ray and neutron diffraction experiments for AgCl, AgI and CuI. For x-ray diffraction, the weights are estimated at $Q = 0$, although in our RMC procedure the Q dependences of the atomic form factors were taken into account.

		Cation–cation	Cation–anion	Anion–anion
CuI	X-ray	0.125	0.450	0.418
	Neutron	0.353	0.482	0.165
AgI	X-ray	0.221	0.498	0.281
	Neutron	0.280	0.498	0.222
AgCl	X-ray	0.539	0.390	0.071
	Neutron	0.146	0.472	0.382

Ag atoms (Ag: 47, I: 53), so the x-ray diffraction emphasizes the correlation including I atoms. This suggests that the peak at around $Q = 1.9$ Å^{-1} in the x-ray diffraction data is mainly attributed to the I–I correlation, while the prepeak at around $Q = 1.0$ Å^{-1} is attributed to the Ag–Ag correlation.

The contributions of three partial structure factors in x-ray and neutron total structure factors are tabulated in table 1 together with those of CuI and AgCl. Reflecting the relatively small difference in the three partial correlations in the HEXED and ND total structures, the differences between the total structure factors of AgI obtained by ND, $S_N(Q)$, and HEXRD, $S_X(Q)$, are not so large compared with differences between those for molten CuI [12] and AgCl [26].

The total pair correlation functions obtained by ND and HEXRD, $g_N(r)$ and $g_X(r)$, have been obtained by conventional Fourier transformation, as shown in figure 2. There are small differences in the height of the first peak and the shape of the second distribution. In typical molten salts, the nearest-neighbour shell is attributed by the unlike-ion correlations. Since, for AgI, x-ray and neutron spectra include almost the same contributions of unlike-ion correlation (see table 1), the higher first peak in $g_N(r)$ suggests that Ag–Ag correlation may give a contribution in the nearest-neighbour range in addition to the unlike pair. On the other hand, the second peak of $g_X(r)$ is higher than that of $g_N(r)$, which suggests that the I–I correlation must contribute to the second peak.

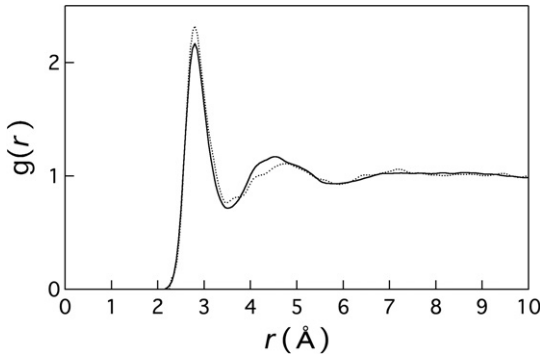

Figure 2. Total pair correlation functions for molten AgI at 650 °C obtained by x-ray (solid line) and neutron (dotted line) diffraction analyses.

Table 2. Number density, box size and cut-off lengths used for RMC simulation. Maximum distances in bond definitions used in statistical analyses of coordination number and bond angle distributions are also shown.

	n_0 (Å^{-3})	Box size (Å)		Cation–cation	Cation–anion	Anion–anion
CuI	0.0282	56.18	Cutoff	1.90	2.10	3.40
			Max distance	3.525	3.1	5.625
AgI	0.0270	56.98	Cutoff	2.25	2.15	2.95
			Max distance	3.61	3.45	5.75
AgCl	0.0380	50.86	Cutoff	2.05	2.00	2.70
			Max distance	several	3.31	5.4

4. Reverse Monte Carlo (RMC) modelling

To see the atomic distribution of molten AgI in detail, the RMC structural modelling [14] has been applied to both the x-ray and neutron structure factor results, simultaneously.

The RMC program creates an atomic configuration model in three-dimensional space reproducing the experimental structure factor, $S_{\mathrm{exp}}(Q)$, and the pair correlation function, $g_{\mathrm{exp}}(r)$. In our modelling procedure, 5000 particles (Ag: 2500, I: 2500) were distributed at random in a cubic box as the initial configuration. The cube sizes were selected to give the proper number density. In addition to these parameters, the applied cut-off distance for each partial correlation and the maximum bond length, which is utilized to define the bonding of the specific atomic pair correlation in the analysis, are listed in table 2 together with those for molten CuI and AgCl reported earlier [12, 26]. The results of the RMC fits to x-ray and neutron diffraction data for molten AgI are shown in figure 1 by the solid line and the chain line, respectively.

As Pusztai and McGreevy pointed out [7], RMC modelling for molten noble-metal halides does not converge to physically reasonable structures when only cut-off constraints are applied. For example, when a loose cut-off length for halogen–halogen correlation is applied, that correlation tends to penetrate into the nearest-neighbour shell, whereas when a severe cut-off length is applied, the halogen atoms tend to be accumulated near the cut-off distance. Both pair correlations are physically unreasonable and unacceptable. This means that ND and XRD total structure factors are not sufficient to generate partial structures in the RMC with the constraint of only cut-off lengths. In such unrealistic structure models, the halogen–halogen distribution tends to show steep structures that are not expected for the halogen–halogen correlation

because, even when taking into account the fact that the unlike pair bonding indicates a covalent character to some extent, the indirect interaction through cation–halogen interaction is in effect among halogen ions. This statement can be justified by the results of theoretical works including empirical and *ab initio* MD [11, 23, 24, 33]. Therefore, the halogen–halogen correlation was dealt with in a special manner in our RMC procedure. After the first RMC modelling with a moderate cut-off length for the halogen–halogen correlation, the shorter side of the first peak of the halogen–halogen correlation was modified to have a Gaussian-like shape and then the second RMC modelling was applied to the ND, XRD experimental total structures and the modified halogen–halogen partial structure. The second RMC run yields slightly better partials in physical meaning but usually they are still unacceptable. Then, after modifying the halogen–halogen correlation again, the next RMC run was carried out. After such iteration, smooth and physically acceptable partials are obtained. The obtained structural model is one of the possible configurations for reproducing the experimental data and the modified halogen–halogen partials that is, to some extent, artificial but physically more reasonable than that generated in the first RMC run. Using the obtained particle configuration, the partial pair correlation functions, the partial structure factors, the coordination number and the bond angle distribution have been analysed.

5. Partial structures and structure model

The partial structure factors of molten CuI, AgI and AgCl obtained by RMC modelling are shown in figure 3. At a glance, the partial structures of molten AgI resemble those of molten CuI but differ from those of molten AgCl.

In the partial structure factors of molten CuI shown in figure 3(a), the I–I correlation, $S^{\mathrm{CuI}}_{\mathrm{I-I}}(Q)$ (hereafter the material is given in the superscript and the correlation in the subscript in the partial functions of the structure factor and pair correlation), causes a prominent sharp peak at $Q = 1.77$ Å^{-1}, followed by a relatively deep valley and an asymmetrical second peak centred at around $Q = 3.1$ Å^{-1}. The Cu–Cu partial structure, $S^{\mathrm{CuI}}_{\mathrm{Cu-Cu}}(Q)$, shows a peak at around $Q = 0.95$ Å^{-1}. In this low-Q region, the FSDP is frequently observed in the structure factor for many structurally disordered materials including amorphous materials and even covalent liquids, which is interpreted to be evidence of medium-range ordering. Although the peak in $S^{\mathrm{CuI}}_{\mathrm{Cu-Cu}}(Q)$ is relatively broad, we describe it as the FSDP hereafter for convenience. The main peak in $S^{\mathrm{CuI}}_{\mathrm{Cu-Cu}}(Q)$ exhibits the shape of a broad hill centred at around $Q = 2.8$ Å^{-1}, which is out of phase relative to $S^{\mathrm{CuI}}_{\mathrm{I-I}}(Q)$. The amplitude of oscillations in $S^{\mathrm{CuI}}_{\mathrm{Cu-Cu}}(Q)$ is extremely small beyond the main peak. These features are completely different from those for molten alkali halides [13]. The cation–cation correlation in a typical molten salt coincides with the anion–anion correlation and is completely out of phase with the unlike-pair correlation, which means that the cation distribution is almost the same as the anion one, and therefore, charge neutrality is maintained locally [13]. For molten CuI, the I–I correlation resembles the halogen–halogen correlation in molten alkali halide, while the Cu distribution must be rather different from the cation distribution in typical molten salts. The unlike-pair partial structure exhibits a deep minimum at around $Q = 1.78$ Å^{-1} where the main peak of $S^{\mathrm{CuI}}_{\mathrm{I-I}}(Q)$ lies, but the first peak does not coincide with any minima of like-pair correlations.

For molten AgI, the I–I structure factor, $S^{\mathrm{AgI}}_{\mathrm{I-I}}(Q)$, has a first peak at around $Q = 1.68$ Å^{-1}, a slightly lower Q position than that in $S^{\mathrm{CuI}}_{\mathrm{I-I}}(Q)$. Except for the lower height of the peak than that in $S^{\mathrm{CuI}}_{\mathrm{I-I}}(Q)$ and an asymmetric tail on the higher Q side of the main peak, the overall profile is similar to that of $S^{\mathrm{CuI}}_{\mathrm{I-I}}(Q)$. The FSDP cannot be recognized in $S^{\mathrm{AgI}}_{\mathrm{Ag-Ag}}(Q)$, in contrast

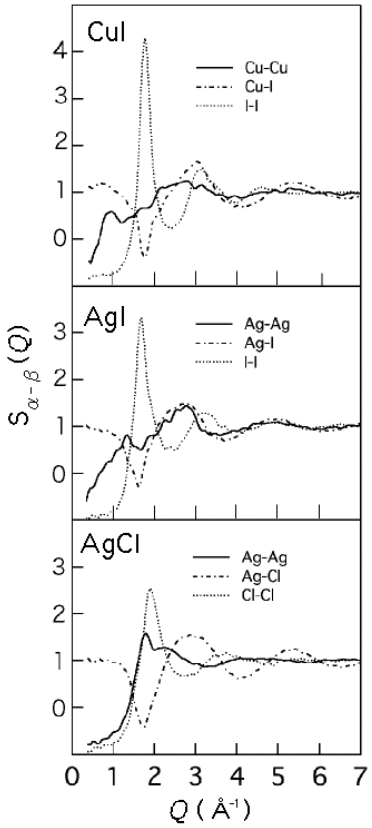

Figure 3. Partial structure factors for molten CuI (upper figure), AgI (middle figure) and AgCl (lower figure). Solid, dotted-chain and dotted lines exhibit cation–cation, cation–anion, and anion–anion correlations, respectively.

to $S^{\mathrm{CuI}}_{\mathrm{Cu-Cu}}(Q)$, but a small peak at $Q = 1.35$ Å^{-1} and a hump-like tail in front of that peak appear. The latter may be a trace of the smeared FSDP. The features in $S^{\mathrm{AgI}}_{\mathrm{Ag-Ag}}(Q)$ in the low-Q region are seen in the partial Ag–Ag structure factor which Shimojo *et al* recently calculated by *ab initio* MD for molten AgI [33], although the small peak lies at a higher Q of around 1.8 Å^{-1}, which coincides with the first peak of $S^{\mathrm{AgI}}_{\mathrm{I-I}}(Q)$. One can distinguish other differences around the middle-Q region in the height and the position of the main peak between our deduced $S^{\mathrm{AgI}}_{\mathrm{Ag-Ag}}(Q)$ and the *ab initio* MD result [33].

$S^{\mathrm{AgI}}_{\mathrm{Ag-I}}(Q)$ has a very similar profile to that of the unlike-pair correlation for molten CuI. However, $S^{\mathrm{AgI}}_{\mathrm{Ag-I}}(Q)$ coincides with $S^{\mathrm{AgI}}_{\mathrm{Ag-Ag}}(Q)$ at $Q > 2$ Å^{-1}, while $S^{\mathrm{CuI}}_{\mathrm{Cu-I}}(Q)$ exhibits an intermediate behaviour between those of $S^{\mathrm{CuI}}_{\mathrm{Cu-Cu}}(Q)$ and $S^{\mathrm{CuI}}_{\mathrm{I-I}}(Q)$. One possible explanation is the difference in ionic radius between the cuprous ion ($Cu^+ \sim 0.96$ Å) and the silver ion ($Ag^+ \sim 1.26$ Å). Another is that the small contrast in the three partial structure factors between XRD and ND data, as shown in table 1, is not enough to distinguish the silver position.

The partial structure factors, $S^{\mathrm{AgCl}}_{\mathrm{Ag-Ag}}(Q)$, $S^{\mathrm{AgCl}}_{\mathrm{Cl-Cl}}(Q)$ and $S^{\mathrm{AgCl}}_{\mathrm{Ag-Cl}}(Q)$, of molten AgCl are shown in figure 3(c). $S^{\mathrm{AgCl}}_{\mathrm{Ag-Ag}}(Q)$ has a broad main peak with a sharp spike at $Q = 1.8$ Å^{-1}, while $S^{\mathrm{AgCl}}_{\mathrm{Cl-Cl}}(Q)$ has a prominent first peak at about $Q = 1.95$ Å^{-1}, which is slightly different

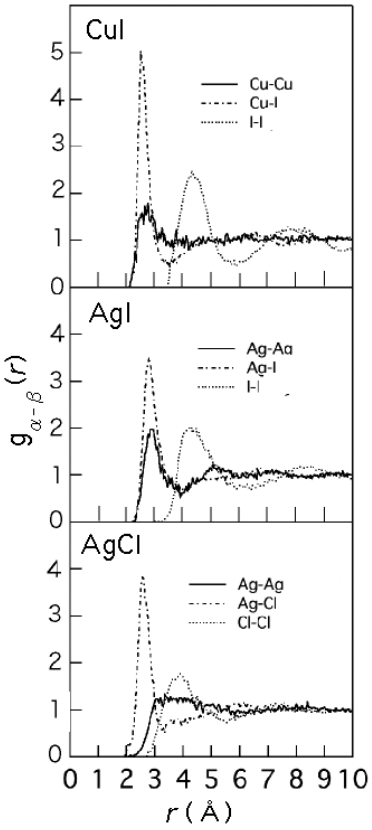

Figure 4. Partial pair correlation functions for molten CuI (upper figure), AgI (middle figure) and AgCl (lower figure). Solid, dotted-chain and dotted lines exhibit cation–cation, cation–anion, and anion–anion correlations, respectively.

from the spike position of $S^{\mathrm{AgCl}}_{\mathrm{Ag-Ag}}(Q)$. The characteristic shoulder seen at around $Q = 2.2$ Å^{-1} in $S^{\mathrm{AgCl}}_{\mathrm{Ag\text{-}Ag}}(Q)$ is consistent with the results of MD simulation including the effects of anion-induced polarization obtained by Trullas *et al* [23] Beyond 4 Å^{-1}, both $S^{\mathrm{AgCl}}_{\mathrm{Ag-Ag}}(Q)$ and $S^{\mathrm{AgCl}}_{\mathrm{Cl-Cl}}(Q)$ look structureless. In contrast to the structure factors for like pairs, $S^{\mathrm{AgCl}}_{\mathrm{Ag-Cl}}(Q)$ exhibits strong oscillations up to $Q = 9$ Å^{-1} beyond the sharp valley at $Q = 1.75$ Å^{-1}. Roughly speaking, the present partial structure factors are similar to the earlier data obtained by Derrien and Dupuy [19] when compared with the envelope of the latter partials, neglecting the noisy spikes that were mistaken as the real structure.

To see the structure in real space, the partial pair correlation functions generated by RMC are shown in figure 4. The partial pair correlation function of Cu–I, $g^{\mathrm{CuI}}_{\mathrm{Cu-I}}(r)$, has a clear and sharp first peak at around 2.58 Å, while, for other peaks beyond the first peak, the amplitude of the oscillation appears almost attenuated (see figure 4(a)). This suggests that the Cu–I interaction is very strong locally. On the other hand, the I–I partial pair correlation function, $g^{\mathrm{CuI}}_{\mathrm{I-I}}(r)$, has periodic oscillations up to 20 Å beyond the first peak at around 4.35 Å, which suggests that the I ions are arranged rather periodically in the middle range even in the liquid state. The Cu–Cu partial pair correlation function, $g^{\mathrm{CuI}}_{\mathrm{Cu-Cu}}(r)$, has a broad peak at around

2.70 Å, which means that the Cu–Cu correlation penetrates into the first unlike-ion coordination shell. This characteristic penetration may be interpreted as a decrease in the Coulomb repulsion force between Cu ions arising from the reduced charge transfer between unlike ions and could be a possible indicator of a partial covalent nature of the Cu–Cu bond [11]. The peak position of $g^{\mathrm{CuI}}_{\mathrm{Cu-Cu}}(r)$ is shifted by 0.2 Å to longer r compared with the AXS results [9], which is consistent with the results of XAFS analysis [10].

In the partial pair correlation function as shown in figure 4 (b), the penetration of the Ag–Ag correlation into the Ag–I nearest-neighbour shell is more significant than that of the Cu–Cu correlation in molten CuI (figure 4(a)). The results of *ab initio* MD simulation [33] suggested a smaller peak. This difference may reflect the differences around the main peak in the structure factors. $g^{\mathrm{AgI}}_{\mathrm{Ag-Ag}}(r)$ exhibits a minimum at around 4 Å, while the Cu–Cu partial pair correlation in molten CuI shows a structureless profile except for the characteristic penetration. The main peak in $g^{\mathrm{AgI}}_{\mathrm{Ag-I}}(r)$ is located at around 2.8 Å. The height of this peak seems relatively low compared with the first peak in $g^{\mathrm{CuI}}_{\mathrm{Cu-I}}(r)$ and even with the *ab initio* MD results for molten AgI [33]; this is associated with the relatively high first peak in $g^{\mathrm{AgI}}_{\mathrm{Ag-Ag}}(r)$. $g^{\mathrm{AgI}}_{\mathrm{I-I}}(r)$ looks very similar to that in the *ab initio* MD results [33], which justifies our treatment of the halogen–halogen correlation in the RMC procedure.

The cation–cation partial pair correlation of molten AgCl is quite different from those of molten CuI and AgI, as shown in figure 4(c). $g^{\mathrm{AgCl}}_{\mathrm{Ag-Ag}}(r)$ shows structureless behaviour, which means that the Ag^+ ions are distributed at random. This property is similar to that of molten CuCl [1, 2]. Although Derrien and Dupuy [19] regarded superimposed oscillations with relatively large amplitude as the real structure and insisted on a difference from molten CuCl, the envelope of their $g^{\mathrm{AgCl}}_{\mathrm{Ag-Ag}}(r)$ result is almost consistent with our data. $g^{\mathrm{AgCl}}_{\mathrm{Ag-Ag}}(r)$ penetrates the first peak of $g^{\mathrm{AgCl}}_{\mathrm{Ag-Cl}}(r)$.

6. Discussions

It was stated, in the previous section, that the main difference between superionic and non-superionic melts is in the cation–cation partial pair correlation. The former exhibits a characteristic penetration into the unlike-pair nearest-neighbour shell and the latter shows an extremely flat correlation. Pusztai and McGreevy [7] suggested that, for molten CuBr, a flat Cu–Cu correlation is possible as a numerical solution, but it violates the physically reasonable cut-off constraints, and that even RMC satisfying the cut-off constraints can create many different partials. Although we do not know whether our treatment for the halogen–halogen partial pair correlation in the RMC procedure is applicable for molten CuBr or not, CuBr is unlikely to have a flat Cu–Cu pair correlation function since molten CuBr must be classified as a superionic melt or as an intermediate between superionic and non-superionic melts.

Distinguishing the differences in an averaged structure is very important. From the atomic configuration obtained by the RMC procedure, the statistics of the bond angles have been analysed as shown in figures 5 and 6. In figure 5, the bond angles for atomic cross-links of M–X–M and X–M–X (M: Cu or Ag; X: Cl or I), $B^{\mathrm{MX}}_{\mathrm{M-X-M}}(\cos(\theta))$ and $B^{\mathrm{MX}}_{\mathrm{X-M-X}}(\cos(\theta))$, are shown for (a) molten CuI, (b) AgI and (c) AgCl. $B^{\mathrm{CuI}}_{\mathrm{I-Cu-I}}(\cos(\theta))$ exhibits a prominent peak centred at about $\cos(\theta) \sim -0.33$; therefore $\theta \sim 110°$, and the number of I atoms coordinated to within 3.1 Å of a central Cu ion is estimated as 2.72, which suggests that the Cu ion is located on the triangular plane formed by three I ions. $B^{\mathrm{CuI}}_{\mathrm{Cu-I-Cu}}(\cos(\theta))$ exhibits a peak at 0.5 corresponding to $\theta \sim 60°$, which results from the penetration of the Cu–Cu partial pair correlation into the Cu–I shell, that is, the Cu–I–Cu triangle with almost the same lengths of Cu–Cu and Cu–I bonds frequently appears. On the other hand, the average number of I

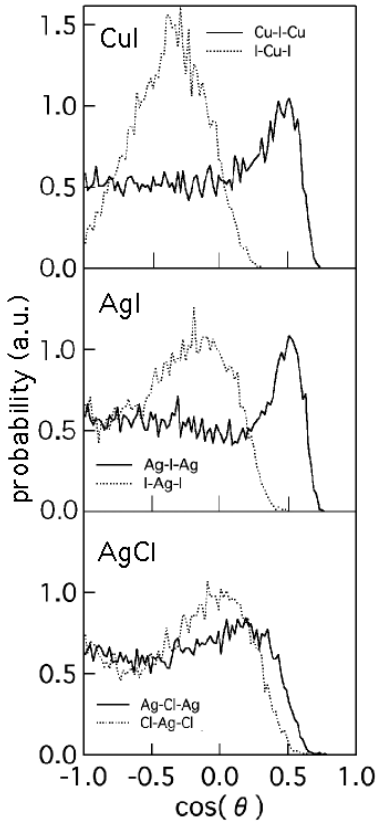

Figure 5. Bond angle distributions of atomic cross-links for molten CuI (upper figure), AgI (middle figure) and AgCl (lower figure). Solid and dotted lines are for cation–anion–cation and anion–cation–anion links, respectively.

ions around a central I ion is 10.9, which suggests that the distribution of I ions is almost a dense random packing. The bond-angle distribution of I–I–I, $B^{\mathrm{CuI}}_{\mathrm{I-I-I}}(\cos(\theta))$, is interpreted in the same manner. The peaks at around 60°, 110° and 180° in the bond-angle distribution are frequent for the dense random packing structure. However, we must keep in mind that $g^{\mathrm{CuI}}_{\mathrm{I-I}}(r)$ has a rather broad first peak compared with the pair correlation of simple liquid metals for which the dense random packing model is a good approximation. On melting, CuI expands by about 20%. When the face-centred-cubic (fcc) structure formed by I ions in α-CuI expands, inhomogeneous expansion may occur. The covalent character of the Cu–I bond can stabilize the triangular unit formed by three I ions.

For molten AgI, a similar interpretation to that in the case of molten CuI can be adopted. $B^{\mathrm{AgI}}_{\mathrm{I-Ag-I}}(\cos(\theta))$ has a broad distribution centred at around -0.17 corresponding to 100°, which is a slightly lower bond angle than that of the peak position in $B^{\mathrm{CuI}}_{\mathrm{I-Cu-I}}(\cos(\theta))$. The number of I ions coordinated within the distance of 3.45 Å to a central Ag ion is estimated to be 3.06. Since the first peak of $g^{\mathrm{AgI}}_{\mathrm{I-I}}(r)$ is similar to that of $g^{\mathrm{CuI}}_{\mathrm{I-I}}(r)$ without any scaling, the large ionic radius of the Ag ion compared with that of the Cu ion may keep the Ag ion slightly further away from the triangular iodine plane compared with the case of molten CuI. The number of I ions around a central I ion is estimated to be 10.95, which is consistent with the value for molten CuI. The similarity between $B^{\mathrm{AgI}}_{\mathrm{Ag-Ag-Ag}}(\cos(\theta))$ and $B^{\mathrm{AgI}}_{\mathrm{I-I-I}}(\cos(\theta))$ is greater than that

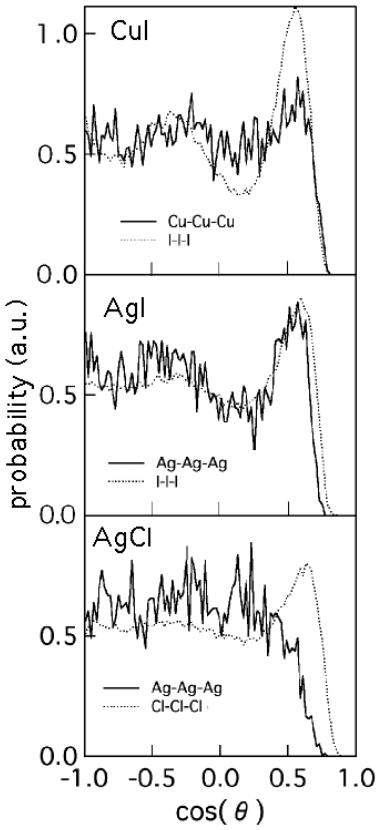

Figure 6. Bond-angle distributions of like-atom links for molten CuI (upper figure), AgI (middle figure) and AgCl (lower figure). Solid and dotted lines are for cation–cation–cation and anion–anion–anion links, respectively.

between $B^{\mathrm{CuI}}_{\mathrm{Cu-Cu-Cu}}(\cos(\theta))$ and $B^{\mathrm{CuI}}_{\mathrm{I-I-I}}(\cos(\theta))$ for molten CuI. The ionic radius of the Ag ion may again be an important factor. It is worth noting that the number density of molten AgI is similar to that of molten CuI, as shown in table 2.

In contrast to superionic melts of molten CuI and AgI, the Ag ion in molten AgCl favours a rock-salt-type local configuration since $B^{\mathrm{AgCl}}_{\mathrm{Cl-Ag-Cl}}(\cos(\theta))$ is distributed at around 0. Because the Ag ionic radius is smaller than the Cl one, the bond angle of Ag–Cl–Ag is slightly smaller, by 10°, than 90°. The average coordination number of Cl ions around a central Ag ion is 3.72, which is less than that of six for the rock-salt structure. The appearance of vacancy sites upon melting may cause the decrease of the coordination number. As expected from the extremely flat Ag–Ag correlation, the bond-angle distribution of Ag–Ag-Ag shows no characteristic feature except for the effect of the excluded volume. $B^{\mathrm{AgCl}}_{\mathrm{Ag-Ag-Ag}}(\cos(\theta))$ with the bond definition of 3.5 Å as the maximum bond length is shown by the solid line in figure 6(c). Changing the bond definition of the maximum bond length from 3 to 4 Å does not result in any modification of $B^{\mathrm{AgCl}}_{\mathrm{Ag-Ag-Ag}}(\cos(\theta))$. On the other hand, the bond-angle distribution of Cl–Cl–Cl has a prominent peak at around 50° and a broad band centred at 115°, which are close to the 60° and 120° for dense random packing. The number of Cl ions around a central Cl ion is estimated to be 12.18.

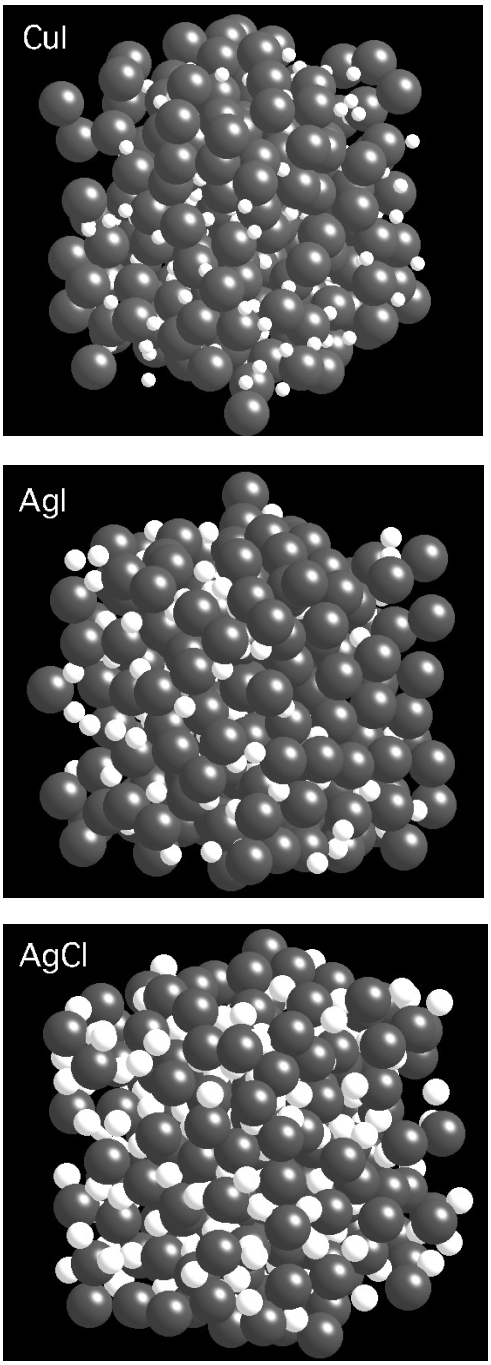

Figure 7. A section (1/8 of the total box in volume) of the atomic configurations obtained by RMC modelling for molten CuI (top), AgI (centre) and AgCl (bottom). White balls denote cations and grey balls denote anions.

The parts of the atomic configurations of molten CuI, AgI and AgCl generated by RMC modelling are shown in figure 7. One can see clear differences in cation distributions between

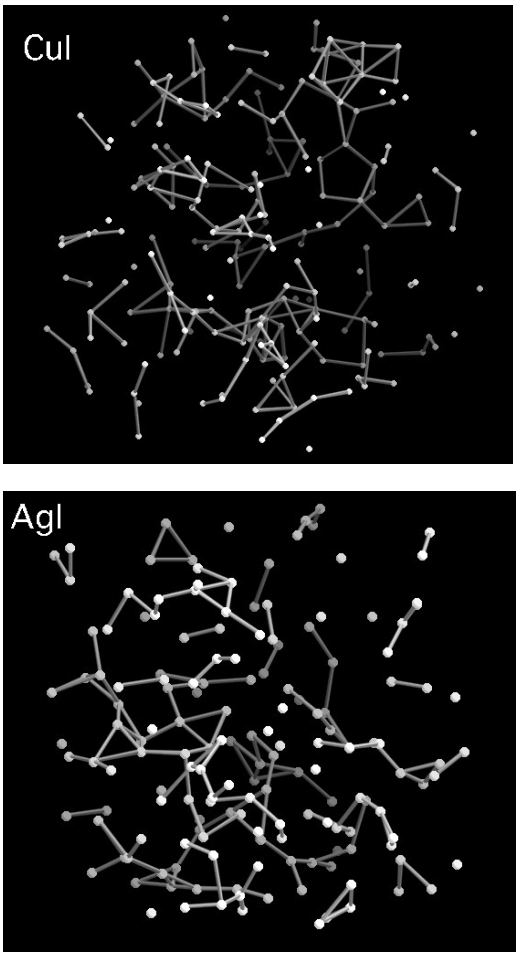

Figure 8. Cation distributions in the model structures for molten CuI (top) and AgI (bottom). Sticks are attached to the neighbouring atoms within 3.525 Å and 3.61 Å, respectively.

superionic ((a) CuI and (b) AgI) and non-superionic ((c) AgCl) melts. The former shows large fluctuations of cations, while the latter exhibits a rather uniform distribution. To see what kind of fluctuations are induced in superionic melts, only cation distributions in molten CuI and AgI are extracted from the atomic configurations shown in figure 7. The successive cations connected to each other according to the bond definitions shown in table 2 seems to partly form a one-dimensional stream (see figure 8), which might be a trace of the cooperative motion of cations due to the slight covalency of cation–cation bonding [11, 33]. To understand the origin of the FSDP, it is helpful to refer to the RMC results for α-CuI by Chahid and McGreevy [34]. They suggested that non-random Cu occupation of tetrahedral vacancy sites in the fcc sublattice formed of immobile iodine ions gives rise to the FSDP at around $Q = 1$ Å^{-1}. In α-CuI, a Cu ion must once enter a spacious octahedral site when it goes from one tetrahedral site to another, since such tetrahedral sites share a corner with each other. In the molten state, I ions can be distributed more uniformly, because the tetrahedral sites are linked by edge and face sharing with each other, as one can see in the atomic configurations shown in figure 7. The one-dimensional stream in the cation distributions means that cations migrate cooperatively

more easily into such closely linked tetrahedral sites. Quasi-elastic neutron scattering spectra of molten CuI [35] exhibit a narrowing at $Q = 0.86$ Å^{-1}. The relaxation time of Cu–Cu correlation at $Q = 0.86$ Å^{-1} was estimated to be 1.6 ps [35]. This result means that mutual diffusion of the Cu–Cu correlation is rather slow in spite of high self-diffusion of Cu ions. Cooperative motion of Cu ions results in a large density fluctuation of Cu ions, which may be the origin of the FSDP in the cation–cation partial structure factor in superionic melts.

In conclusion, differences can be distinguished in the local environment and cation distribution between superionic melts of CuI and AgI and non-superionic melt of AgCl. The main features of superionic melts are the penetration of the cation–cation partial distribution into the nearest-neighbour shell of unlike-pair and a large fluctuation in the cation distribution. When cations within the distance of the bond definitions are linked with each other (see figure 8), they form a one-dimensional stream, which may demonstrate the cooperative motion of cations. In the non-superionic melt of AgCl, the Cl–Ag–Cl link favours 90°, but Cl atoms are arranged in a dense random packing that favours threefold and sixfold symmetry. This mismatch seems to be cause of the flat structure of the Ag–Ag correlation. Whether such local structure is common in other non-superionic melts such as molten CuCl and AgBr is still open to discussion.

7. Summary

For molten AgI, high-energy x-ray diffraction and neutron diffraction measurements have been performed. Reverse Monte Carlo modelling has been applied to these structural data and the obtained detailed partial structures based on the atomic configuration have been discussed in comparison with the recently reported results for molten CuI [12] and AgCl [26]. The cation–cation distributions in CuI and AgI exhibit a penetration into the nearest-neighbour shell of the unlike-atom correlation, while that of molten AgCl shows a flat correlation. The analysis of the distributions of bond angles and coordination numbers revealed that the cation is located on the triangular plain formed by three iodine ions in CuI and AgI, while AgCl favours the right angle for the Cl–Ag–Cl link. This means that the local environment in each solid phase just before melting is retained. The cation distributions in superionic melts of CuI and AgI exhibit large fluctuations, while Ag ions in the non-superionic melts of AgCl are distributed much more uniformly.

Acknowledgments

The authors appreciate helpful discussions with Professors M Silbert, F Shimojo and P S Salmon. ND experiments were performed at KENS with the approval of KEK (proposal numbers 2001-B2-61) and HEXRD experiments were performed at SPring-8 with approval of JASRI (proposal number 2005A0711-ND1c-np). This work was partly supported by a Grant-in-Aid for Creative Scientific Research (No. 16GS0417) from the Ministry of Education, Culture, Sports, Science and Technology of Japan.

References

[1] Page D I and Mika K 1971 *J. Phys. C: Solid State Phys.* **4** 3034
[2] Eisenberg S, Jal S F, Dupuy J, Chieux P and Knoll W 1982 *Phil. Mag.* A **46** 195
[3] Stafford A J, Silbert M, Trullás J and Giró A 1990 *J. Phys.: Condens. Matter* **2** 6631
[4] McGreevy R L and Pusztai L 1990 *Proc. R. Soc.* A **430** 241
[5] Shirakawa Y, Saito M, Tamaki S, Inui M and Takeda S 1991 *J. Phys. Soc. Japan* **60** 2678

[6] Allen D A and Howe R A 1992 *J. Phys.: Condens. Matter* **4** 6029
[7] Pusztai L and McGreevy R L 1998 *J. Phys.: Condens. Matter* **10** 525
[8] Saito M, Park C, Omote K, Sugiyama K and Waseda Y 1997 *J. Phys. Soc. Japan* **66** 633
[9] Waseda Y, Kang S, Sugiyama K, Kimura M and Saito M 2000 *J. Phys.: Condens. Matter* **12** A195
[10] Trapananti A, Di Cicco A and Minicucci M 2002 *Phys. Rev.* B **66** 014202
[11] Shimojo F, Aniya M and Hoshino K 2004 *J. Phys. Soc. Japan* **73** 2148
[12] Takeda S, Fujii H, Kawakita Y, Kato Y, Kohara S and Maruyama K 2006 *Physica* B **385/386** 249
[13] For example Edwards F G, Enderby J E, Howe R A and Page D I 1975 *J. Phys. C: Solid State Phys.* **8** 3483
Biggins S and Enderby J E 1982 *J. Phys. C: Solid State Phys.* **15** L305
Mitchell E W J, Poncet P F J and Stewart R J 1976 *Phil. Mag.* B **34** 721
Locke J, McGreevy R L, Messoloras S, Mitchell E W J and Stewart R J 1985 *Phil. Mag.* B **51** 301
[14] McGreevy R L and Pusztai L 1988 *Mol. Simul.* **1** 359
[15] Boyce J B and Huberman B A 1979 *Phys. Rep.* **51** 189
[16] Hull S and Keen D A 1996 *J. Phys.: Condens. Matter* **8** 6191
[17] Shimojo F and Aniya M 2003 *J. Phys. Soc. Japan* **72** 2702
[18] Madden P A and Wilson M 2000 *J. Phys.: Condens. Matter* **12** A95
[19] Derrien J Y and Dupuy J 1976 *Phys. Chem. Liq.* **5** 71
[20] Inui M, Takeda S, Shirakawa Y, Tamaki S, Waseda Y and Yamaguchi Y 1991 *J. Phys. Soc. Japan* **60** 3025
[21] Keen D A, Hayes W and McGreevy R L 1990 *J. Phys.: Condens. Matter* **2** 2773
[22] Wilson M, Madden P A and Costa-Cabral B J 1996 *J. Phys. Chem.* **100** 1227
[23] Trullàs J, Alcaraz O, González L E and Silbert M 2003 *J. Phys. Chem.* B **107** 282
[24] Bitrián V and Trullàs J 2006 *J. Phys. Chem.* B **110** 7490
[25] Saito M, Kang S, Sugiyama K and Waseda Y 1999 *J. Phys. Soc. Japan* **68** 1932
[26] Tahara S, Fujii H, Kawakita Y, Kohara S, Yokota Y and Takeda S 2007 *J. Non-Cryst. Solids* **353** 1994
[27] Isshiki M, Ohishi Y, Goto S, Takeshita K and Ishikawa T 2001 *Nucl. Instrum. Methods* A **467/468** 66
[28] Fukunaga T, Misawa M, Fujikawa I and Satoh S 1993 *KENS Report* vol 9, p 16
[29] Suzuki K, Misawa M, Kai K and Watanabe N 1977 *Nucl. Instrum. Methods* **147** 519
[30] Paalman H H and Pingth C J 1968 *J. Appl. Phys.* **33** 1075
[31] Blech I A and Averbach B L 1965 *Phys. Rev.* A **137** 1113
[32] Sears V F 1992 *Neutron News* **3** 26
[33] Shimojo F, Inoue T, Aniya M, Sugahara T and Miyata Y 2006 *J. Phys. Soc. Japan* **75** 114602
[34] Chahid A and McGreevy R L 1998 *J. Phys.: Condens. Matter* **10** 2597
[35] Kawakita Y, Kato Y, Shigeta H, Shibata K and Takeda S 2007 *J. Alloys Compounds* at press